Journal of the Indian Institute of Science
A Multidisciplinary Reviews Journal
ISSN: 0970-4140 Coden-JIISAD

REVIEWS

Phase-Field Modelling of Solidification Microstructures

Mathis Plapp

ABSTRACT | Phase-field models have become the most popular method for the numerical simulation of solidification microstructures. This is due to several reasons: (i) they are based on thermodynamic principles, which facilitate their application in metallurgy, (ii) they are numerically simple, and standard mathematical methods for the solution of partial differential equations can be employed, and (iii) they can be very accurate, which has been demonstrated by number of benchmark simulations. In order to be both accurate and efficient, the dynamics of the interfaces in the model has to be precisely controlled. This is achieved by the construction of the model, and demonstrated by matched asymptotic expansion methods. Here, some fundamentals of phase-field modelling will be introduced, and several examples of their application in the modelling of solidification microstructures will be reviewed.

Keywords: *modelling, microstructure, solidification, thermodynamics*

1 Introduction

Solidification is a phenomenon that is commonly observed in our daily environment. It is also one of the oldest processes used by mankind to obtain high-performance materials: in the bronze age and the iron age, new knowledge about metallurgical processes drove major progress in civilizations. Later on, steelmaking was one of the motors of the industrial revolution, and only the capacity to grow high-purity silicon crystals has made modern microelectronics possible. Therefore, solidification is a traditional and important subject in materials science.

The solidification of materials generally leads to the spontaneous emergence of *microstructures*: domains of different phases or grains of different orientation are delimited by interfaces and grain boundaries, respectively. These microstructures originate from the processes that take place at the crystallization front. The growth of the solid requires transport of heat and chemical components to/from the interface. This limitation of growth by transport leads to morphological instabilities: a planar growing interface is unstable, hills and valleys appear, and finally the solid-liquid interface can take very complicated shapes. The most well-known example are probably dendrites, tree-shaped structures whose main branches grow in crystallographic directions and are decorated by many sidebranches (see Figure 1). Microstructure formation is an example of *pattern formation* outside of equilibrium,[1] that is, the emergence of a complicated structure from a simple initial state (the liquid). In this perspective, it is interesting to understand theoretically this self-organization process, in order to predict which kind of structure is formed for a given material under given processing conditions.

The study of solidification phenomenon in the light of the modern theory of pattern formation started in the 1980s[2] and has been ongoing ever since. A large body of knowledge about solidification microstructures has been accumulated.[3–5] This is useful for the design of new materials, since the initial structuration during solidification influences many materials properties, even though solidification is generally followed by other processing steps (rolling, machining, heat treatments, etc.).

Microstructures are shaped by non-equilibrium processes, and are consequently *not* equilibrium shapes. Therefore, knowledge about the *interface*

Laboratoire de Physique de la Matière Condensée, École Polytechnique, CNRS, Université Paris-Saclay, 91128 Palaiseau, France.
Mathis.Plapp@polytechnique.fr

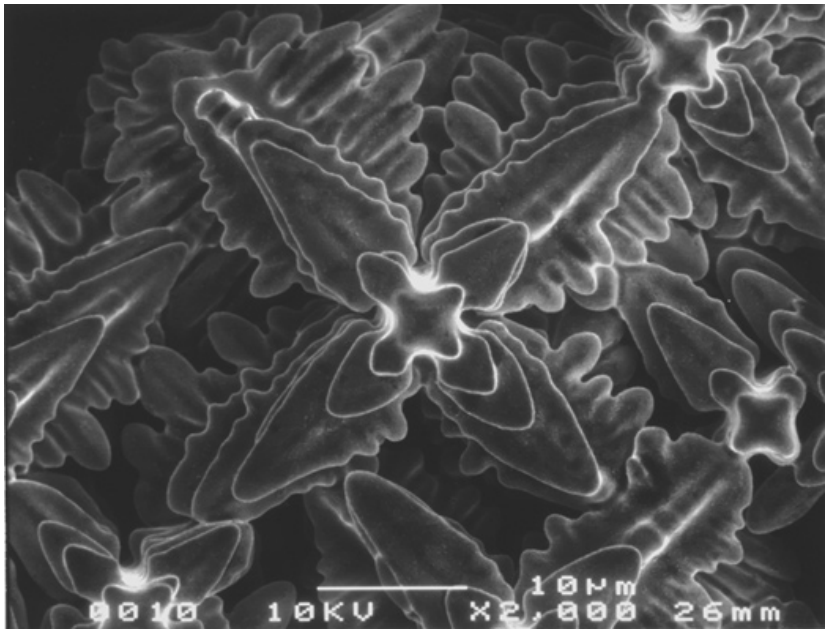

Figure 1: Dendrites that cover the wall of a hot tear in a CMSX4 Nickel-based superalloy (SEM picture, courtesy of W. Kurz and S. Mokadem, EPFL Lausanne, Switzerland, 2003).

dynamics is necessary for a complete understanding of microstructure formation. Such information can be obtained from in situ experiments or from numerical simulations. Direct comparison of experiments and simulations is particularly useful, both to validate the numerical models and to elucidate the details of the pattern-formation process.

The phase-field method has become the "standard method" for numerical simulations of solidification microstructures in recent years.[6,7] Its fundamental principle is to represent the geometry of microstructures by one or several scalar functions, the *phase fields* (named so, because they indicate which thermodynamic phase is present at each point in space). These continuous fields take constant values in the bulk of each phase, and exhibit smooth but rapid variations through the interfaces. In many cases, the phase fields can be indentified with an *order parameter* that describes a particular phase transition. The dynamics of the interfaces is governed by an equation of motion for the phase field that is coupled to the relevant transport equations for heat and/or chemical components.

A phase-field model is a set of coupled non-linear partial differential equations of a form that is quite standard—it can also be interpreted as a set of reaction-diffusion equations. Therefore, a wide range of numerical methods is available to perform simulations, including parallel algorithms that can work on modern high-performance architectures.

Reaction-diffusion équations: Set of partial differential équations which describes the time evolution of the concentrations of a set of chemical species that can react with each other or be transported by molecular diffusion.

As a consequence, it is straightforward to implement and run a phase-field model. However, care has to be taken during the *construction* of the model, that is, in the formulation of the model equations, because seemingly small differences in the equations can have a big impact on the model performance.

In order to understand this fact, let us discuss in somewhat more detail the physical scales that are involved in the problem of microstructure formation. In most metals, the solid-liquid interfaces are rough on an atomic scale, that is, the transition between the ordered solid and the disordered liquid takes place gradually over a distance of several atomic spacings (see for example the molecular dynamics studies reviewed in Ref.[8]). Since atoms can easily attach and detach from the crystal in this situation, the interface exhibits strong fluctuations. Therefore, a description of this interface in terms of a continuous order parameter seems well justified (see also[9]). The "physical" interface thickness is thus of the order of 1 nm. On the other hand, microstructures are named after their characteristic scale, which is the micron. For example, dendrite tip radii in typical metallurgical samples are of the order of 10 μm; an entire dendritic grain can be millimeters in diameter.

As a consequence, it is impossible to use phase-field models with realistic physical parameters for the simulation of microstructures. Indeed, in any continuum model in which a field has a variation on

the scale of 1 nm, the grid spacing has to be of that order (at least inside the interfaces), which means that an enormous number of grid points would be required to simulate even a simple microstructure. The only viable path is to use models in which the "numerical" interface thickness is much larger than the thickness of the physical interfaces. The construction of the model needs to take this perspective into account: Only models in which the interface thickness can be "upscaled" without introducing numerical artefacts will be useful for numerical simulations. This means that the physics of the diffuse interfaces in the model needs to be carefully controlled.

The physics of the problem (conservation laws, symmetries etc.) can give certain guidelines for the construction of the model. But if the model is to be used for simulations that match a particular substance, a prescription has to be given that allows the user to properly choose the model parameters. That is, a precise relation between the parameters of the model and the physical parameters of the studied problem needs to be established. The standard procedure to achieve this is to use the mathematical technique of *matched asymptotic expansions* (also sometimes called boundary layer method). Its principle is to analyze the mathematical problem on the two different scales already introduced above, that is, the interface scale (inner scale) and the microstructure scale (outer scale). On each scale, a perturbation analysis is carried out, and the two expansions are matched. In this way, the solution of the interface (inner) equation will provide the boundary conditions that apply on the outer scale.

In the remainder of this article, I will first introduce the traditional way of formulating the problem of solidification in terms of sharp interfaces, and comment on its justification (Sec. 2). Then, I will give an introduction to the phase-field method, discuss its relation to the sharp-interface formulation and describe some applications to simple systems, in Sec. 3. I will then conclude and outline some perspectives in Sec. 4.

2 Sharp-Interface Formulation

Historically, one of the first mathematical descriptions of a phase-change problem was given by Josef Stefan,[10,11] who considered the growth of a flat (planar) layer of ice on the surface of a pool of water in contact with cold air. He chose to represent the interface between water and ice by a mathematical surface (with thickness zero and without internal structure), and solved the heat transport equation in the solid and applied a boundary condition at the moving solid-liquid interface. Later on, it was formally proven that this problem was well-posed, and mathematicians often call this type of problems "Stefan problems".[12] A more general term is *free-boundary problem*, which stresses the fact that in such problems, the spatial domain in which a partial differential equation has to be solved is not fixed, but evolves with time. Moreover, the domain shape is itself a part of the solution. It is for this reason that free-boundary problems are notoriously hard to solve, both analytically and numerically. Nevertheless, they give a very intuitive picture of the crystal growth process, and therefore it is useful to present this formulation first.

As outlined above, "physical" interfaces in metals are not sharp and have an internal structure. The sharp-interface formulation nevertheless is appropriate because of the separation of scales that was already discussed: seen on the scale of an entire dendrite, the interfaces indeed "look sharp". Actually, there is a rigorous justification of this formulation, which will be briefly outlined now.

2.1 *Planar interface in equilibrium*

Consider a heterogeneous system in equilibrium that exhibits a planar interface (normal to the x direction) between two phases α and β. For simplicity, several assumptions are made. First, elastic effects in the solid phase will be neglected in all that follows. A more complete treatment of interface equilibrium with elasticity can be found, for example, in Ref.[13] Next, the two phases are assumed to have the same total number density (or, equivalently, the same molar volume). That is, if the system is made of K different chemical components, and $\rho_i(z)$ is the number density of component i (in atoms or molecules per unit volume) at position x (since the interface is planar, a one-dimensional treatment is sufficient), we have

$$\sum_{i=1}^{K} \rho_i(x) = \bar{\rho}, \tag{1}$$

where the constant total number density $\bar{\rho} = N_A/V_m$, with N_A the Avogadro number and V_m the molar volume. The (dimensionless) compositions are defined as

$$c_i(x) = \frac{\rho_i(x)}{\bar{\rho}}, \tag{2}$$

which obviously implies that $\sum_{i=1}^{K} c_i(x) = 1$.

The assumption of constant molar volume has several important consequences. First, since the two phases have the same number density, interface

Grid spacing: The simplest method for the numerical integration of a partial differential equation is to discretize it on a regular grid in space and time. The distance between two consecutive grid points is called the grid spacing. It sets the minimal length that can be resolved by the computation.

Hydrodynamic motion: The macroscopic (hydrodynamic) velocity is defined as the local average of the molecular velocities. In an AB mixture, even if this average velocity is zero, the concentrations of the species can evolve in time due to exchange of A and B atoms. This corresponds to diffusion.

motion can take place without hydrodynamic motion (only diffusive processes are required). Second, the Helmholtz free energy density (per unit volume) and the Gibbs free energy (per mole of substance) are simply related by the constant $\bar{\rho}$: $f = F/V = \bar{\rho}\, G/N$, where F and G are the Helmholtz and Gibbs free energies, respectively, V is the total volume and N the total number of particles. This means that either of these two free energies can be used. In the following, mainly F, and its volume density f will be used. Volume densities of other extensive thermodynamic quantities are also defined, such as the entropy density $s = S/V$ and the internal energy density $e = U/V$.

Extensive quantities: In thermodynamics, countable quantities that vary with the system size if the state of matter is held constant (for example, energy or number of particles).

Intensive quantities: In thermodynamics, the quantities that describe the state of matter and that are independent of the size of the system (for example, temperature).

Thermodynamic equilibrium between two phases α and β implies that all intensive quantities must be equal in the two phases. Those intensive variables are the pressure P, the temperature T, and the chemical potentials μ_i defined by

$$\mu_i = \left.\frac{\partial F}{\partial N_i}\right|_{V,T,N_j}. \qquad (3)$$

The pressure can be expressed as the negative of the grand potential density, $P = -(f - \sum_{i=1}^{K} \mu_i \rho_i)$. Therefore, the equality of the pressures in the two phases yields

$$f^{\alpha} - \sum_{i=1}^{K} \mu_i \rho_i^{\alpha} = f^{\beta} - \sum_{i=1}^{K} \mu_i \rho_i^{\beta}, \qquad (4)$$

where the superscripts α and β indicate that the quantity is evaluated in the respective phase. Two special cases are detailed for future reference. For a pure substance ($K = 1$), $P^{\alpha} = P^{\beta}$ implies $f^{\alpha} = f^{\beta}$ according to Eq. (1). For a binary alloy ($K = 2$), one of the number densities can be eliminated. Setting $\rho = \rho_2$ yields

$$f^{\alpha} - \rho^{\alpha}(\mu_2 - \mu_1) = f^{\beta} - \rho^{\beta}(\mu_2 - \mu_1). \qquad (5)$$

Only the difference of the two chemical potentials appears in this expression. This is quite natural: under the constraint of constant number density, the numbers of the constituent molecules cannot be varied independently, so that an increase in N_1 is always accompanied by a decrease in N_2. The quantity $\mu = \mu_2 - \mu_1$, thus, describes the exchange of components, and is often called the *diffusion potential*.

One additional remark is useful here: with the definition of Eq. (3), chemical potentials and diffusion potentials have a dimension of energy. In much of the phase-field (and more generally, materials science) literature those quantities are introduced with a dimension of energy per unit volume. This results from the definition $\mu = \partial f/\partial c$. Since the molar Gibbs free energy is related to the chemical potentials, $G = V_m \sum_{i=}^{K} \rho_i \mu_i$, the so-defined diffusion potential can also be seen as the volume density of a modified Gibbs free energy. For constant molar volume, these two different conventions are strictly equivalent, but this issue will need to be carefully reconsidered for variable molar volume.

Whereas intensive quantities are the same in the two phases, the densities of extensive quantities vary. For example, for a solid-liquid interface in a pure substance, the internal energy density and the entropy density are not the same on the two sides of an interface. The typical profile of an arbitrary extensive quantity y across a diffuse interface is depicted in Fig. 2: its density smoothly varies between the two bulk values. The question then arises as to how to define the exact position of the interface. One solution is given by the well-known *Gibbs construction*: the total content of the extensive quantity that is contained in the system is compared to the same quantity in a fictitious system that exhibits a discontinuous jump between the bulk values (the profile across the interface is a step function). Mathematically, for a system of total length L this is expressed by the integral

$$\delta y = \left(\int_0^L y(x)\, dx\right) - \left[y^{\alpha} x_{\text{int}} + y^{\beta}(L - x_{\text{int}})\right], \qquad (6)$$

where x_{int} is the position of the step. The interface position can then be *defined* by the requirement $\delta y = 0$.

Two remarks are in order. First, in general there are several extensive quantities that exhibit a jump through the interface. There is no reason that the interface positions defined with their

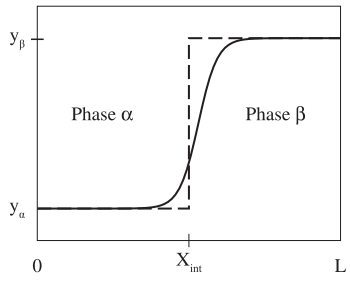

Figure 2: Illustration of the Gibbs construction: Thermodynamic properties and a position on a macroscopic scale can be assigned to a diffuse interface by comparing the total content of an extensive quantity $y(x)$ with the one of a step function, localized at the position x_{int}.

respective profiles coincide. In this situation, one quantity is chosen as a reference, and the δy of the other extensive quantities remain non-zero. This can be seen as an *interface excess* of the respective quantities. Second, if $y^{\alpha} = y^{\beta}$, the excess δy is independent of the choice of x_{int}; in particular, it cannot be eliminated. The most important such quantity is the *interface excess free energy* γ. For a pure substance, this reads

$$\gamma = \int_0^L [f(x) - f_{eq}]\, dx, \tag{7}$$

where $f_{eq} = f^{\alpha} = f^{\beta}$ is the bulk equilibrium free energy density (the same in the two phases according to Eq. (5)). For a binary alloy,

$$\gamma = \int_0^L [\omega(x) - \omega_{eq}]\, dx, \tag{8}$$

where $\omega = f - \rho\mu$ and ω_{eq} its equilibrium value. This excess is always positive and non-zero because the creation of a surface or interface always has a free energy cost when compared to a homogeneous phase.

2.2 *Curved interfaces in equilibrium*

The interface excess free energy plays a central role in the equilibrium of curved surfaces. In particular, it leads to the Gibbs-Thomson effect, which will be briefly reviewed now.

In the sharp-interface picture, the total free energy of a two-phase system is given by the sum of the bulk free energies and the interfacial free energy,

$$F = \int_{V_\alpha} f_\alpha(\vec{x})d\vec{x} + \int_{V_\beta} f_\beta(\vec{x})d\vec{x} + \oint_S \gamma(n)d\vec{S}, \tag{9}$$

where V_α and V_β are the spatial domains occupied by the phases α and β, respectively, f_α and f_β are the free energy densities of the two phases that may depend on the position $\vec{x}$ through its variables (in particular, the composition), S is the domain boundary separating α and β (the interface), $\hat{n}$ is the unit normal vector to the interface pointing into the β phase, and $d\vec{S}$ is a surface element. The interface free energy γ may depend on the orientation on the surface as soon as at least one of the phases is crystalline. Indeed, the presence of the crystallographic structure breaks the isotropy in space, and many properties of the surface may depend on its orientation with respect to the crystallographic axes (for example, the number of "broken bonds" per unit surface).

For a two-phase system to be in equilibrium, the variation of the above free energy with respect to the position of the two-phase boundaries must be zero. Several cases, of increasing complexity, will now be detailed. Consider first a solid crystallite inside a liquid in two dimensions at a constant temperature T. Suppose in addition that the surface free energy is isotropic. This implies that the shape of the crystallite should be a sphere (a circle in two dimensions). Since, at constant temperature, the free energy densities of solid and liquid are just constants, the above free energy simply becomes

$$F = F_0 + [f_s(T) - f_l(T)]\pi R^2 + 2\pi R\gamma, \tag{10}$$

where R is the radius of the crystallite, and F_0 is the free energy of the system completely filled with liquid at temperature T. Variation with respect to R yields

$$\delta F = 2\pi\{[f_s(T) - f_l(T)]R + \gamma\}. \tag{11}$$

Since γ and R are positive, this variation can only be zero if $f_s(T) - f_l(T)$ is negative, which is the case for $T < T_m$ with T_m the melting temperature. The free energy densities may be expanded around T_m to yield

$$f_\nu \approx f_\nu(T_m) + \left.\frac{\partial f_\nu}{\partial T}\right|_{T_m} (T - T_m) \qquad (\nu = l, s). \tag{12}$$

For a pure substance, $f_s(T_m) = f_l(T_m)$ according to Eq. (5). The derivative of the free energy density with respect to the temperature is the negative of the entropy density ($\partial f/\partial T = -s$), and the latent heat of melting per unit volume is defined as

$$L = T_m(s_l - s_s). \tag{13}$$

Combining these relations yields the Gibbs-Thomson law,

$$T = T_m - \frac{\gamma T_m}{L}\frac{1}{R}. \tag{14}$$

In addition to this "energetic" point of view, there is a "mechanical" one. Indeed, in the absence of elastic interactions, the surface free energy is equivalent to the surface tension, that is, one may associate to γ a tensile force that is tangential to the surface. For curved surfaces, the balance of forces on a small piece of surface $d\ell$ yields a resulting force of magnitude γ/R that is directed towards the center of curvature and that generates a pressure difference between "outside" and "inside". Application of thermodynamic relations then again yields Eq. (14).

Broken bonds: In the simplest model of a crystal, the atoms are linked by rigid chemical bonds that have a fixed energy. If the crystal is cut into two parts, bonds have to be broken, and the number of broken bonds times the bond energy is an estimate for the interface energy. The number of broken bonds per unit surface depends on the lattice structure and the orientation of the cut surface.

For anisotropic interfaces, γ depends on the orientation $\hat{n}$ (in two dimensions, $\hat{n}$ is equivalent to an angle θ with respect to one of the crystallographic axes). It is often written as

$$\gamma(\hat{n}) = \bar{\gamma} a_c(\hat{n}). \tag{15}$$

Wulff construction: The Wulff construction proceeds as follows: (i) draw a polar plot of the surface tension as a function of orientation, (ii) for each direction, draw the normal to the radius vector at the distance from the center that corresponds to the value of the surface tension, and (iii) take the inner envelope of all the normals (normal planes in three dimensions). The result is the equilibrium shape.

The variational problem is more complicated since the shape of the crystallite is no longer a sphere. The problem of finding the equilibrium shape is solved geometrically by the *Wulff construction*; the result is that Eq. (14) is replaced in two dimensions by

$$T = T_m - \frac{\bar{\gamma} T_m}{L} \frac{a_c(\theta) + a_c''(\theta)}{R}, \tag{16}$$

where a_c'' denotes the second derivative of the function $a_c(\theta)$ with respect to θ. Since the temperature remains constant and a_c varies with orientation, R is no longer a constant—it is the local radius of curvature defined by $1/R = \partial\theta/\partial s$ with s the arclength, along the interface. There is also a "mechanical" interpretation of the new term (proportional to a_c''): for anisotropic interfaces, there is not only a tension along the interface, but also a torque (since the surface can lower its energy by "turning" towards a more favorable orientation). On a curved surface, the differential between the torques acting on the ends of a surface element $d\ell$ generates an additional resulting force that is added to the tensile force.

In three dimensions, the interface is a two-dimensional surface, which implies that it can be rotated in two linearly independent directions. The second derivative of a_c becomes a matrix, and the curvature becomes a tensor, the eigenvalues of which are the principal curvatures. The Gibbs-Thomson condition reads

$$T = T_m - \frac{\bar{\gamma} T_m}{L} \sum_{i=1,2} \left(a_c(\hat{n}) + \frac{\partial^2 a_c}{\partial \theta_i^2} \right) \frac{1}{R_i}, \tag{17}$$

where R_i are the principal radii of curvature and $\partial^2/\partial\theta_i^2$ are the second derivatives along the corresponding principal directions. Whereas this formula looks complicated, one should keep in mind that it follows naturally from the variation of the free energy given in Eq. (9). For isotropic interfaces, $1/R$ in Eq. (14) is simply replaced by $2/R$ (there are two directions of curvature).

For binary alloys at a fixed temperature T, the only intensive quantity that can vary in response to the interface curvature is the diffusion potential. In order to fully exploit the equivalence between the intensive variables (temperature and diffusion potential), it is advantageous to switch to the thermodynamic potential $\Omega = F - \mu N$, which for a two-phase system reads

$$\Omega = \int_{V_\alpha} \omega_\alpha(\vec{x}) d\vec{x} + \int_{V_\beta} \omega_\beta(\vec{x}) d\vec{x} + \oint_S \gamma(\hat{n})\, d\vec{S}, \tag{18}$$

where $\omega_v = f_v - \mu\rho_v$ are the Legendre transforms of the free energy densities. This transform corresponds to a change of variables from the number density (or composition) to the diffusion potential. Note that, at equilibrium, $\omega_\alpha = \omega_\beta$ according to Eq. (5), and that the surface free energy is defined as the interface excess of this potential. The potential Ω has been called grand potential,[14,15] which is not entirely correct (the grand potential density is $f - \sum_{i=1}^{K} \mu_i \rho_i$, with μ_i the chemical potentials); however, for constant molar volume, this potential has all the properties of the grand potential. In particular, it is minimized at equilibrium, and it satisfies

$$\rho = \bar{\rho} c = -\frac{\partial \omega}{\partial \mu}. \tag{19}$$

Repeating the steps leading from Eq. (9) to (14) yields for an inclusion of the β phase in an α matrix

$$\mu = \mu_{\text{eq}} + \frac{\gamma}{\rho_\beta - \rho_\alpha} \frac{1}{R} \tag{20}$$

for isotropic interfaces. Here, μ_{eq} is the equilibrium diffusion potential for α-β coexistence (with a planar interface) at temperature T. The difference in sign of the curvature term with respect to Eq. (14) comes from the fact that the definition of the latent heat in Eq. (13) contains $s_l - s_s$, which would be equivalent to $\rho_\alpha - \rho_\beta$. Obviously, for anisotropic interfaces the same generalizations of the right-hand side as for a pure substance must be made. It is more customary to write the above equation in terms of composition, which yields

$$c_\nu - c_\nu^{\text{eq}} = \frac{\gamma}{f_\nu''(c_\nu^{\text{eq}})(c_\beta^{\text{eq}} - c_\alpha^{\text{eq}})} \frac{1}{R} \tag{21}$$

where $\mu = \partial f/\partial\rho$ has been used, and f'' denotes $\partial_2 f/\partial c$.[2] Here, c_ν^{eq} is the equilibrium composition of phase ν for coexistence at μ_{eq}.

2.3 *Moving interfaces*

While the equilibrium of interfaces is controlled by the intensive quantities, the balance of extensive

quantities controls the interface motion. Indeed, since the density of extensive quantities varies across an interface, an interface can only move if the difference is supplied by a transport process. This idea can be formalized by formulating a balance law for an arbitrary extensive quantity in a box that is fixed at (and moves with) the interface. Indeed, consider a piece of interface of surface area A, and draw a box that encloses the interface as well as a small portion of the adjacent space, centered at the interface and with a width of $2d$ in the direction normal to the interface. We can write the balance of an arbitrary extensive quantity that satisfies a conservation law, by counting the fluxes that cross the box boundaries, and by taking into account the motion of the box. At fixed surface area, the fluxes parallel to the interface can be neglected for d sufficiently small, since the corresponding faces of the box become negligibly small.

Consider a planar interface of a pure substance that moves in the x direction with velocity V. The change of total energy in the box writes

$$\frac{dE}{dt} = A\big[-j_l(x_{\text{int}}+d) + j_s(x_{\text{int}}-d) + V\left(e_l(x_{\text{int}}+d) - e_s(x_{\text{int}}-d)\right)\big], \qquad (22)$$

where $j_\nu = -\lambda_\nu \partial_x T$ is the heat flux, λ_ν being the heat conductivity in phase ν, and the terms proportional to V represent the internal energy that enters the moving box at the front and leaves it at the back, respectively. Two steps are necessary to obtain the so-called *Stefan condition*: the limit $d \to 0$ must be taken, which means that all quantities are evaluated on the two sides of the (sharp) interface. Moreover, a steady state is considered, such that the time derivative of the energy in the box must be zero. This yields

$$V(e_l - e_s) = j_l - j_s = -\lambda_l \left.\frac{\partial T}{\partial x}\right|_l + \lambda_s \left.\frac{\partial T}{\partial x}\right|_s. \qquad (23)$$

This equation thus, just expresses the heat balance at the moving interface.

To close the problem, the internal energy densities must be specified as a function of the interface state. Most commonly, these conditions are stated for the temperature rather than for the internal energy. For solid-liquid systems, one assumes that the temperature on the two sides of the interface is the same. However, this temperature depends on the velocity of the interface. Indeed, interface motion is a dissipative process, and therefore, a driving force is necessary to generate motion. A simple linear ansatz yields

$$V = \mu_k (T_{\text{eq}} - T_{\text{int}}), \qquad (24)$$

where the sign is chosen such that a growing solid corresponds to a positive velocity, and μ_k is the interface mobility (this notation is quite common in the literature; not to be confused with the diffusion potential μ). Combining this with Eq. (14) yields the generalized Gibbs-Thomson relation,

$$T = T_m - \frac{\gamma T_m}{L}\frac{1}{R} - \frac{V}{\mu_k}. \qquad (25)$$

Many different theories have been formulated to predict the kinetic coefficient μ_k, and its value has been determined in molecular dynamics simulations (it is impossible to measure it directly in experiments); see for example Ref.[16] and references therein for a recent summary. Obviously, the growth kinetics of a crystal can depend on the orientation of the interface, which makes μ_k anisotropic.

For alloys, mass balance needs to be satisfied in addition to energy balance. A calculation completely analogous to the one above for the energy yields for a binary alloy

$$V(c_l - c_s) = -D_l \left.\frac{\partial c}{\partial x}\right|_l + D_s \left.\frac{\partial c}{\partial x}\right|_s, \qquad (26)$$

with D_ν the solute diffusion coefficient in phase ν. Again, the compositions at the interface have to be specified to close the problem. The situation in alloys is more complicated than for pure substances, because local equilibrium at the interfaces can break down. Indeed, when solidification is driven by rapid extraction of heat, solute diffusion is not fast enough to establish the equilibrium solute concentrations at the interface: *solute trapping* occurs, that is, the solute is "trapped" by the rapidly advancing solidification front. In the extreme case, the liquid solidifies without change in composition (massive transformation). As soon as solute trapping occurs, there is a jump in the diffusion potential across the interface (in the analogy with a pure substance, this would correspond to a temperature jump). In this situation, a theory is needed which gives the two interface diffusion potentials (or equivalently the two interface compositions) as a function of velocity. The classic theory of solute trapping is the continuous growth model of Aziz,[17] but a complete understanding of this phenomenon is still lacking. Therefore, the examples discussed in the remainder of this article will all be chosen in the regime of sufficiently slow solidification, such that the local equilibrium at the interfaces is maintained. In this situation, the diffusion potential is the same on the two sides of

the interface, and the equilibrium relation between the compositions on the two sides remains valid. Obviously, the finite interface mobility μ_k has also to be included for alloy solidification.

Before proceeding to the concrete examples, let us reflect on the developments seen above. In fact, implicitly, the concept of scale separation was used in the derivation of the Stefan condition. Namely, Equation (22) is valid for an arbitrary interface, with or without internal structure. In contrast, in Eq. (23) the limit of zero box thickness was taken. Obviously, for a "physical" diffuse interface with a finite thickness W, this structure would become "visible" in the Stefan law as soon as $d < W$. In particular, there is no guarantee that the heat currents and the internal energy densities are sufficiently smooth to define the differentials on the right-hand side of Eq. (23). As a consequence, the interface thickness should explicitly appear in the equation. The validity of Eq. (23), which is independent of the interface thickness, therefore, rests on the assumption that the "external" fields (temperature and composition) are sufficiently smooth on the scale of W. This condition is *not* fulfilled in the case of solute trapping: the main parameter of the Aziz theory is the ratio WV/D_i, where D_i is a solute diffusion coefficient in the interface. The interface compositions therefore explicitly depend on the interface structure. Very similar considerations will be crucial for the interpretation of phase-field models.

2.4 *Symmetric model for pure substance solidification*

A particularly simple model is the *symmetric model of solidification*, in which certain thermodynamic properties and transport coefficients are assumed to be the same in liquid and solid. In particular, the specific heat C and the thermal diffusion coefficient D_{th} are taken as identical. This makes it possible to transform the equation of heat conservation in the bulk,

$$\partial_t e = -\vec{\nabla}\cdot\vec{j} = \vec{\nabla}(\lambda\vec{\nabla}T), \tag{27}$$

into a diffusion equation for the temperature, using $de = CdT$ and $\lambda = CD_{th}$,

$$\partial_t T = D_{th}\vec{\nabla}^2 T. \tag{28}$$

Dilute binary alloy: A binary mixture in which one sort of atoms (say, B) is much less frequent than the other. A and B are called solvent and solute, respectively.

Since the specific heats of the two phases are identical, the latent heat is independent of temperature, and the Stefan condition simply reads

$$LV_n = D_{th}\hat{n}\cdot\left[-\vec{\nabla}T\Big|_l + \vec{\nabla}T\Big|_s\right], \tag{29}$$

where $\hat{n}$ is the unit normal vector pointing into the liquid, V_n is the (signed) normal velocity of the interface, and the temperature gradients are evaluated on the two sides of the interface. Finally, the temperature at the interface obeys the generalized Gibbs-Thomson condition,

$$T_{\text{int}} = T_m - \frac{\overline{\gamma}T_m}{L}\sum_{i=1,2}\left(a_c(\hat{n}) + \frac{\partial^2 a_c}{\partial\theta_i^2}\right)\frac{1}{R_i} - \frac{V_n}{\mu_k}. \tag{30}$$

For convenience, a non-dimensional temperature field is introduced

$$u = \frac{T - T_m}{L/C}, \tag{31}$$

where the ratio L/C has the dimension of temperature. In terms of this variable, the free-boundary problem reads

$$\partial_t u = D_{th}\vec{\nabla}^2 u, \tag{32}$$

$$V_n = D_{th}\hat{n}\cdot\left[-\vec{\nabla}u\Big|_l + \vec{\nabla}u\Big|_s\right], \tag{33}$$

$$u_{\text{int}} = -d_0\sum_{i=1,2}\left(a_c(n) + \frac{\partial^2 a_c}{\partial\theta_i^2}\right)\frac{1}{R_i} - \beta V_n, \tag{34}$$

where we have introduced the thermal capillary length

$$d_0 = \frac{\overline{\gamma}T_m C}{L^2} \tag{35}$$

and the interface kinetic coefficient

$$\beta = \frac{C}{L\mu_k}. \tag{36}$$

This formulation will be particularly helpful in establishing the connection with the phase-field model.

2.5 *One-sided model for solidification of a dilute binary alloy*

A general sharp-interface model for alloy solidification can be written down, but for simplicity attention will be restricted here to the case of a dilute binary alloy made of substances A and B, with a simple phase diagram: straight liquidus and solidus lines of slopes m and m/k, respectively, ($m < 0$), where k is the partition coefficient. The interface is supposed to be in local equilibrium, that is,

$$c_s = kc_l, \tag{37}$$

where c_s and c_l are the compositions at the solid and liquid side of the interface, respectively. This *partition relation* is equivalent to the statement that the diffusion potential is the same on both sides of the interface. The number density of B atoms is noted ρ, and $c = \rho/\bar{\rho}$.

The interface temperature satisfies the generalized Gibbs-Thomson relation,

$$T = T_m - |m| c_l - \frac{\gamma T_m}{L}\frac{1}{R} - V_n/\mu_k, \tag{38}$$

where T_m is the melting temperature of pure A. Note that the isotropic version of the Gibbs-Thomson condition was used for simplicity of notation; the anisotropic version of the curvature term is identical to the one in Eq. (30).

For substitutional solutes, diffusion is generally much slower in the solid than in the liquid. In the *one-sided* model of solidification, solute transport in the solid is completely neglected. Heat is supposed to diffuse much faster than solute, so that the temperature field can be taken as fixed by external conditions, in spite of the rejection of latent heat during solidification. Then, Eq. (38) yields a boundary condition for the solute concentration at the interface.

For isothermal solidification at a fixed temperature $T_0 < T_m$, the above assumptions lead to the set of sharp-interface equations

$$\partial_t c = D\vec{\nabla}^2 c, \tag{39}$$

$$(c_l - c_s)V_n = c_l(1-k)V_n = -D\hat{n}\cdot\vec{\nabla}c\,|_l, \tag{40}$$

$$m(c_l - c_l^{\mathrm{eq}}) = \frac{\gamma T_m}{L}\frac{1}{R} + \frac{V_n}{\mu_k} \tag{41}$$

where D is the solute diffusivity in the liquid, and $c_l^{\mathrm{eq}} = (T_0 - T_m)/m$ the equilibrium concentration of the liquid at T_0.

A close analogy with the pure substance model can be obtained by rewriting the above equations in terms of the local supersaturation with respect to c_l^{eq}, normalized with the equilibrium concentration gap at T_0,

$$U = \frac{c - c_l^{\mathrm{eq}}}{c_l^{\mathrm{eq}}(1-k)}. \tag{42}$$

This results in

$$\partial_t U = D\vec{\nabla}^2 U, \tag{43}$$

$$[1 + (1-k)U]V_n = -D\vec{\nabla}U\,|_l, \tag{44}$$

$$U = -\frac{d_0}{R} - \beta V_n, \tag{45}$$

where d_0 and β are the chemical capillary length and kinetic coefficient: the temperature scale L/C of Eqs. (35) and (36) is replaced by the freezing range $\Delta T_0 = |m|(1-k)c_l^{\mathrm{eq}}$, which yields $d_0 = \gamma T_m/(L\Delta T_0)$, and $\beta = 1/[\mu_k \Delta T_0]$.

The notation U is used here to distinguish the dimensionless supersaturation field from the dimensionless temperature field u introduced previously, but they play perfectly analogous roles. Actually, it can be shown that the field U is a dimensionless diffusion potential.[14,18] For a constant concentration gap ($k = 1$), a one-sided version of the pure substance model is obtained. Finally, directional solidification can also be treated by replacing the constant temperature field by an externally imposed temperature gradient of magnitude G along the z direction that moves with a velocity V_p with respect to the material (sample) frame,

$$T(z) = T_0 + G(z - V_p t). \tag{46}$$

Then, a term $-(z - V_p t)/l_T$ has to be added to the right-hand side of Eq. (45), where $l_T = \Delta T_0/G$ is the thermal length (see[18] for details).

3 Phase-Field Models

3.1 *Introduction*

The free-boundary formulation is appealing because it directly corresponds to our intuition about the motion of macroscopic domains—the finite thickness of the interfaces is hidden from our eyes or even the standard means of observation (for example, optical microscopes). Of course, this very fact is also the reason why sharp-interface models are an excellent description: there is a scale separation of several orders of magnitude between the thickness of the interface and the characteristic length scales of the macroscopic problem, such that the internal structure of the interfaces has no detectable effect on the macroscopic evolution. There are two different approaches for the numerical treatment of such problems: front tracking and front capturing. In front-tracking methods, the interface location is described by marker points that move with the interfaces (see Figure 3). For structures that develop complicated shapes, this poses several methodological challenges: the spacing between marker points changes with time, so that remeshing becomes necessary. When the connectivity of the structure changes (pinchoff or coalescence), the points have to be re-ordered. As a result, front-tracking codes are complicated. An alternative is interface capturing, in which the position of the interface

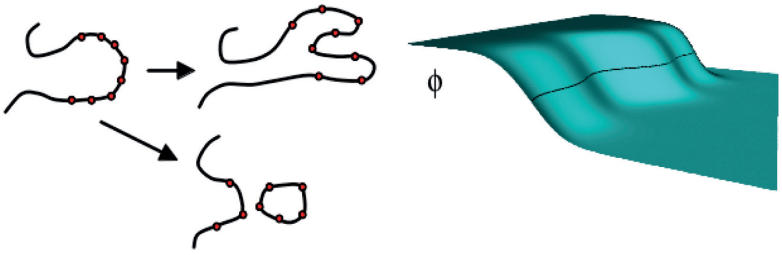

Figure 3: Illustration of interface tracking versus interface capturing methods: in interface tracking (left), the interface is represented *explicitly*, for example by marker points. In interface capturing (right), it is treated *implicitly* as a level set of a function that evolves with time (black line on the blue surface).

is described by the level set of an auxiliary function.

The name *phase field* was coined in the beginning of the 1980s when the first diffuse-interface models for solidification were formulated.[19–21] These models are rooted in the physics of phase transitions. Their origins can be traced back to the continuum description of liquid-gas interfaces developed by van der Waals,[22] and to the Landau theory of phase transitions. Indeed, the latter introduces the concept of *order parameters*, which are descriptors of phase transitions, and in the 1970's, equations of motion for such order parameters were developed to describe the dynamics of phase transitions.[23] In this "bottom-up" perspective, the phase field and its dynamics can be obtained by a coarse-graining procedure from a microscopic model by eliminating the atomistic degrees of freedom, but retaining the degrees of freedom that correspond to mesoscopic scales. These concepts have been exposed in many treatments, see for example[6,7,24]. Whereas this approach is very useful for the understanding of the roots of the phase-field method, it is impossible to apply it to the treatment of concrete problems since the coarse-graining procedure can hardly ever be carried out explicitly (for an attempt on a simple lattice model, see Ref.[25]).

Order parameters: A phase transition always involves an ordered and a disordered phase (the entropy changes discontiuously). An order parameter is a quantity that is zero in the disordered phase and non-zero in the ordered phase. Order parameters may be scalars, vectors, or tensors. For example, in ferromagnets, the magnetization is zero above the Curie temperature, but finite below.

Coarse-graining: Heterogeneous systems may be treated by introducing a length scale, the coarse-graining length. All quantitites are averaged over the coarse-graining length (for example, by dividing space in boxes), but variations on larger scales are kept. Generally, the results depend on the choice of the coarse-graining length.

For these reasons, I have adopted in the following, the opposite "top-down" approach in which phase-field models are seen as a phenomenological tool to treat free-boundary problems such as the ones exposed in the preceding section. Whereas a purely mathematical treatment is possible, models that remain rooted in thermodynamics have the advantage, as will be seen below, to contain "automatically" the right physics, in particular the Gibbs-Thomson effect. It turns out that the combination of physical structure and mathematical analysis is the best way to obtain models that are both accurate and efficient. In this perspective, the phase field is seen as a mathematical tool for the computation of the interface evolution, and its equation of motion only needs to reproduce, on a large scale, the desired free-boundary problem.

The phase field is a scalar field that specifies the local state of matter (solid or liquid). Its direct interpretation as an order parameter in the spirit of Landau theory is difficult, since the solid-liquid phase transition does not exhibit a critical point; however, various definitions have been explored.[9,26] Here, it will be interpreted rather as being related to the local volume fraction of the solid phase, that is, the phase field ϕ is 0 in the liquid and 1 in the solid. Between these two values in the bulk phases, the phase field varies smoothly across a diffuse interface, like an extensive quantity as depicted in Fig. 2. As a consequence, the phase field can also be used to interpolate thermodynamic and kinetic properties across the interface.

3.2 *Solidification of a pure substance*

In the top-down point of view, a phase-field model can be seen as a a *regularization* of the free-boundary problem. Indeed, the sharp-interface equations implicitly contain singularities: the materials properties (for example specific heat, diffusion coefficient) exhibit jumps at the interface, and the surface free energy is concentrated on a infinitely thin sheet, which makes its volume density infinite. In the Stefan boundary condition of Eq. (29), the latent heat is released at the infinitely thin interface, which corresponds to a singular heat source term. Formally, this can be made apparent by rewriting the equations in terms of distributions: the domain occupied by the solid is represented by an indicator function, $\theta_s(\vec{x})$, which equals 1 inside the solid, and zero outside. The interface location can then be described by a Dirac δ function that is related to the derivative of θ_s, $\vec{\nabla}\theta_s = -\delta(\vec{x}-\vec{x}_{\mathrm{int}})\hat{n}$, where $\hat{n}$ is again the unit normal to the interface pointing into the liquid, and $\vec{x}_{\mathrm{int}}$ is any point located on the interface.

Detailed discussions about this procedure can be found in.[5,27–30]

In a phase-field model, these singularities are *smoothed out*. The free energy of Eq. (9) for a two-phase system may be approximated for a pure substance by

$$F = \int_V f_{\text{int}}(\phi, \vec{\nabla}\phi) + g(\phi) f_s(T) + (1 - g(\phi)) f_l(T). \tag{47}$$

Here, f_{int} represents the surface energy contribution, equal to zero outside of the interfaces, and is discussed in detail below, $f_s(T)$ and $f_l(T)$ are the free energy densities of solid and liquid, respectively, and $g(\phi)$ is an interpolation function that satisfies

$$g(0) = 0 \quad g(1) = 1 \quad g'(0) = g'(1) = 0. \tag{48}$$

The two choices that are most frequently used in the literature are the polynomials $g(\phi) = 3\phi^2 - 2\phi^3$ and $g(\phi) = 10\phi^3 - 15\phi^4 + 6\phi^5$. The motivation for Eq. (47) is easily understood: both of the quoted expressions for $g(\phi)$ are monotonous in ϕ, and therefore $g(\phi(\vec{x}))$ is an approximation for the step function $\theta_s(\vec{x})$, and $g(\phi)f_s(T)+(1 - g(\phi))f_l(T)$ approximates the bulk free energy in the sharp-interface formulation.

Equations of motion for the phase field ϕ and the temperature T may be obtained by considering the variations of the free energy. Since the crystalline order can change locally by short-range motion of the atoms into or out of the equilibrium positions in a crystal lattice, the phase field is a locally non-conserved quantity. Therefore, according to linear response theory, it satisfies a simple relaxation dynamics,

$$\partial_t \phi = -\Gamma \frac{\delta F}{\delta \phi}, \tag{49}$$

where Γ is a kinetic constant and $\delta F/\delta\phi$ is the variational derivative of the functional (47). This equation just states that matter will tend to adopt the state with the lowest free energy.

Away from the interfaces, where f_{int} is zero, the equation becomes

$$\partial_t \phi = -\Gamma g'(\phi)[f_s(T) - f_l(T)], \tag{50}$$

and the last condition in Eq. (48), $g'(0) = g'(1) = 0$, ensures that the bulk equilibrium values of the phase field are always equal to 0 or 1. Indeed, the two fixed points of this equation are $\phi = 0$ and $\phi = 1$, even when $T \neq T_m$, and thus, $f_s \neq f_l$. This is *not* the case for the simplest choice $g(\phi) = \phi$ that was adopted in the early phase-field models.[19,21]

The equation for the temperature can be obtained with the help of thermodynamic identities. The variation of the free energy with respect to the temperature is the negative of the entropy density. Since f_{int} is assumed to be independent of temperature,

$$\frac{\delta F}{\delta T} = -s(T, \phi) = -s_s(T) g(\phi) - s_l(T)[1 - g(\phi)], \tag{51}$$

where $s_v = -\partial f_v(T)/\partial T$ are the entropy densities of liquid and solid. At constant density (equivalent to locally constant volume, and thus to the absence of mechanical work), $de = Tds$, which yields

$$de = T\frac{\partial s}{\partial T} dT + T\frac{\partial s}{\partial \phi} d\phi \tag{52}$$

with the help of the chain rule. Since the specific heat $C = T\partial s/\partial T$ and the latent heat $L = T[s_l(T) - s_s(T)]$, a combination of the above equation with the energy conservation law, Eq. (27), gives

$$C(\phi, T)\partial_t T = \vec{\nabla}(C(\phi, T) D \vec{\nabla} T) + L g'(\phi) \partial_t \phi. \tag{53}$$

In the case of the symmetric model, C is independent of ϕ. In a limited range of temperatures around the melting point, the values of C, s_s, s_l, and L may be approximated by their values at the melting point. This results in the simple equation,

$$\partial_t T = \vec{\nabla}(D\vec{\nabla} T) + \frac{L}{C} g'(\phi) \partial_t \phi, \tag{54}$$

which is very intuitive: the temperature changes by heat diffusion in the bulk, and by the release of latent heat at the interface. The equation for the phase field can also be simplified by expanding the free energies in the right hand side around the melting temperature, which yields

$$\frac{1}{\Gamma}\partial_t \phi = (\text{interface part}) - g'(\phi)\frac{L}{T_m}(T - T_m). \tag{55}$$

3.3 *Interface structure and energy*

The interface free energy density f_{int} is of the general form suggested by Ginzburg-Landau theory, with a gradient square term and a local potential,

$$f_{\text{int}} = \frac{K}{2}\left(\vec{\nabla}\phi\right)^2 + H f_{\text{dw}}(\phi). \tag{56}$$

Here, $f_{dw}(\phi)$ is a function of ϕ that has two minima of value $f_{\text{dw}} = 0$ for $\phi = 0$ and $\phi = 1$, with a maximum in between these two values

Linear response theory: Standard method in statistical mechanics to obtain a relation between thermodynamic forces and fluxes. The macroscopic evolution is obtained by averaging over microscopic events, using the equilibrium fluctuation spectrum. The resulting force-flux relations are always linear, with coefficients that may depend on temperature.

Ginzburg-Landau theory: The Ginzburg-Landau theory was originally developed as a description of the transition from the normal to the superconducting state, and later generalized to other phase transitions.

(a double-well potential), and K and H are constants. A simple dimensional analysis immediately clarifies the role of these constants: since f_{int} is a free energy density (of dimension energy/volume), H has the same dimension (f_{dw} is a dimensionless function), whereas K has dimension of energy/length. Therefore, the combination

$$W = \sqrt{\frac{K}{H}} \tag{57}$$

has the dimension of length and indicates the width of the diffuse interface, whereas $\sqrt{KH}$ has the dimension of a surface tension. The two coefficients K and H thus, determine the width and the excess free energy of the interface.

For a more detailed view, it is useful to recall the general prescription for calculating the variational derivative of a free-energy integral with a free-energy density $f(\phi, \vec{\nabla}\phi)$,

$$\frac{\delta F}{\delta \phi} = \frac{\partial f}{\partial \phi} - \sum_{i=1}^{d} \frac{\partial}{\partial x_i} \frac{\partial f}{\partial(\partial_i \phi)}, \tag{58}$$

where d is the dimension of space, and i labels the coordinate directions (x, y, z in three dimensions). A planar interface at rest at the melting temperature T_m is an equilibrium state and must therefore, satisfy $\delta F/\delta\phi = 0$. Indeed, for $T = T_m$ the bulk driving force is zero according to Eq. (55), and only the interface contribution remains. Application of Eq. (58) to the free energy density f_{int} of Eq. (56) yields

$$0 = -K\partial_{xx}\phi + H\, f'_{\mathrm{dw}}(\phi) \tag{59}$$

for an interface normal to the x direction. One may divide this equation by H and switch to the dimensionless variable $\tilde{x} = x/W$ with W defined by Eq. (57), which yields

$$\partial_{\tilde{x}\tilde{x}}\phi = f'_{\mathrm{dw}}(\phi). \tag{60}$$

This indicates that the interface profile is entirely determined by the choice of f_{dw}, whereas the spatial scale of the profile is set by W. Furthermore, according to Eq. (7), the surface free energy is defined as the integral of the interface excess of the free energy,

$$\begin{aligned}\gamma &= \int_{-\infty}^{\infty} f_{\mathrm{int}}\, dx \\ &= H\int_{-\infty}^{\infty}\left[\frac{1}{2}W^2\left(\partial_x\phi\right)^2 + f_{\mathrm{dw}}(\phi)\right]dx \\ &= \sqrt{KH}\int_{-\infty}^{\infty}\left[\frac{1}{2}\left(\partial_{\tilde{x}}\phi\right)^2 + f_{\mathrm{dw}}(\phi)\right]d\tilde{x}.\end{aligned} \tag{61}$$

In the last expression, the integral is dimensionless (a number that will be called I in the following) and can be evaluated by inserting the solution of Eq. (60). As a result, the surface energy γ is given by

$$\gamma = I\sqrt{KH} = IWH, \tag{62}$$

where Eq. (57) was used to obtain the second expression, which is particularly intuitive. Indeed, H is the amplitude of the double-well potential, that is, it gives the height of the energy barrier between the two equilibrium phases. The product of this barrier height and the thickness of the interface thus gives the total interface excess energy. In the sharp-interface limit ($W \to 0$), the interface free energy density has to diverge ($H \to \infty$) in order to maintain a finite γ. This corresponds to one of the singularities of the free-boundary problem.

The phenomenological coefficients K and H can therefore be expressed in terms of two physical quantities: the interface thickness and the surface energy. The result is

$$H = \frac{\gamma}{IW} \qquad K = \frac{\gamma W}{I}. \tag{63}$$

If the physical values of both γ and W are used, the values of K and H are close to those obtained by mean-field theories for phase transitions.[24] However, in the "top-down" point of view, W can be treated as a free parameter since it does not appear in the free-boundary problem. In many articles on phase-field modelling, K and H are directly expressed in terms of W and γ in the free-energy functional. Note, however, that the number I depends on the choice of the double-well potential, and that different numerical prefactors appear in the literature since the definition of the interface width is not unique (the definition given here corresponds to the notations of Karma and Rappel,[31] but other choices are equally legitimate and have been used). The most common choice for the double-well potential is $f_{\mathrm{dw}} = \phi^2(1-\phi)^2$, for which Eq. (60) yields $\phi(\tilde{x}) = (1/2)[1 - \tanh(\tilde{x}/\sqrt{2})]$ (for a solid located in the domain $x < 0$).

In order to include anisotropy, that is, generate a surface free energy that depends on the interface orientation according to Eq. (15), Eq. (63) can still be used, but the coefficients K and/or H need to be orientation-dependent. The interface orientation (unit normal vector pointing into the liquid) is given in terms of the phase field by

$$\hat{n} = -\frac{\vec{\nabla}\phi}{|\vec{\nabla}\phi|}. \tag{64}$$

Historically, anisotropy was first included in the gradient energy coefficient,[32–34] $K(\hat{n}) = \bar{K} a_c(\hat{n})^2$, since the gradient has vector character. According to Eq. (57), this creates variations in the interface thickness W, which becomes proportional to a_c. A constant interface thickness is obtained by letting $K(\hat{n}) = \bar{K} a_c(\hat{n})$ and $H(\hat{n}) = \bar{H} a_c(\hat{n})$. Finally, it is also possible to keep the gradient energy coefficient constant and to write $H(\hat{n}) = \bar{H} a_c^2(\hat{n})$, which leads to $W \sim 1/a_c(\theta)$. It should be noted that each of these choices generates different equations of motion for the phase field, since the second term on the right-hand side of Eq. (58) acts on any $\hat{n}$-dependent term in the functional.

3.4 *Relation to sharp-interface models*

In order to make the phase-field model useful as a tool for the numerical simulation of free-boundary problems, the equivalence between the phase-field model and the free-boundary problem needs to be established. Since the equation for the temperature is based on the same transport equation for heat as in the standard transport theory, in the bulk the two models are clearly identical. It remains to be demonstrated that the phase-field model generates the correct boundary conditions at the interfaces, and to relate the parameters of the phase-field model to those of the free-boundary problem.

The general strategy to achieve this is presented below; to begin with, let us examine two simple ingredients: the equilibrium Gibbs-Thomson relation and the Stefan condition. In Sec. 2.2, the Gibbs-Thomson condition was obtained by setting the variation of the appropriate two-phase free energy to zero. Since the functional used in the phase-field model, Eq. (47), is a smoothed version of the very same free energy, it is easy to see that the phase-field model automatically contains the Gibbs-Thomson effect. Indeed, consider first the isotropic case, with a spherical inclusion of solid in the liquid. As long as the radius of the inclusion is much larger than the interface thickness W, the interface profile will remain close to the solution for a planar interface, which means that the surface energy is unaltered. Then, a variation in R corresponds to a shift of the entire interface profile, which changes the amount of the two bulk phases and the length of the interfaces in the same way as in the sharp-interface formalism. For anisotropic interfaces, the new terms generated by the action of the functional derivative on the anisotropy function $a_c(\hat{n})$ represent the torque exerted by anisotropy; the application of the prescription given by Eq. (58), thus produces the physically correct anisotropic Gibbs-Thomson condition, Eq. (17).

Consider now a planar solid-liquid interface that grows with constant velocity V. For slow motion (such that the diffusion length, D/V, is much larger than the interface thickness W), the temperature is almost constant on the scale of W, and therefore, the left-hand side of Eq. (54) is small compared to the last term of the right-hand side, which contains the rapidly varying phase field. The two terms on the right-hand side must therefore, balance each other. In the frame that moves with the interface (this transformation replaces ∂_t with $-V\partial_x$), Eq. (54) with its left-hand side set to zero reads

$$0 = \vec{\nabla}(D\vec{\nabla}T) - V\frac{L}{C}g'(\phi)\partial_x\phi. \tag{65}$$

Since $g(\phi)$ varies from 1 in the solid to 0 in the liquid, an integration of this equation across the interface directly yields the Stefan condition, Eq. (29).

A more formal proof, and at the same time a more general treatment, is provided by the technique of *matched asymptotic expansions*, often also called boundary-layer calculations. The main steps of such a formal calculation are the following.

1. Define two different coordinate systems. The first one corresponds to the sharp-interface problem ("outer scale"), characterized by a macroscopic scale ℓ specific to the considered problem (in the previous examples, the radius of curvature and the diffusion length, respectively). The second ("inner scale") is attached to the interface (in general in a curvilinear moving coordinate system), and scaled by the interface thickness W. The ratio $\varepsilon = \ell/W$ defines a small parameter.
2. Expand formally the relevant fields (here, phase field and temperature) as a power series in the parameter ε on the two different scales, which gives an outer expansion and an inner expansion.
3. Solve the equations of the phase-field model perturbatively order by order in ε in each region, using the relevant coordinate system.
4. Match the two expansions order by order using the condition that the limit of the inner expansion far from the interface must coincide with the limit of the outer expansion when the interface is approached.

The result of this procedure are boundary conditions for the relevant fields on the outer scale, which are determined by the equations on the

inner scale. In general, these boundary conditions also take the form of a power series in ε. The explicit calculation of the matched asymptotics is quite tedious and is presented in detail in several publications.[18,31,35,36] It is therefore, not discussed in detail here. The principles and main results are illustrated in the forthcoming section for one specific model, which is the celebrated model of Karma and Rappel.[31]

3.5 *Example: The Karma-Rappel model*

The model proposed by Karma and Rappel was the first example for the successful application of the "top-down" approach, that is, quantitative simulations of dendritic growth were performed, with results that were largely independent of the interface thickness. This model can be obtained from the general formalism introduced above by the following steps and choices:

1. Choose $f_{dw} = 4\phi^2(1-\phi)^2$ and $g(\phi) = 10\phi^3 - 15\phi^4 + 6\phi^5$.
2. Replace the function $g(\phi)$ by another function $h(\phi)$ in the equation for the temperature, Eq. (54). This function describes how the latent heat is released inside the interface, and should therefore, satisfy $h(0) = 0$ and $h(1) = 1$. If $h(\phi) \neq g(\phi)$, the model is no longer variational; however, it has been shown in[31] that more efficient models can be obtained with this additional freedom. The simplest choice is $h(\phi) = \phi$.
3. Change variables from ϕ to $\psi = (1+\phi)/2$ (which thus is equal to 1 in the solid and −1 in the liquid) and from T to the dimensionless field u introduced in Eq. (31). Divide the equation for the phase field by the constant H contained in f_{int}, define the phase-field relaxation time by $\tau = 1/(\Gamma H)$, and combine all constants and numerical prefactors in the last term on the right-hand side in a dimensionless coupling parameter λ.

This results in the following two simple equations, written here for simplicity for the case of isotropic interface energy and mobility:

$$\tau \partial_t \psi = W^2 \vec{\nabla}^2 \psi + \psi - \psi^3 - \lambda u (1-\psi^2)^2, \qquad (66)$$

$$\partial_t u = D\vec{\nabla}^2 u + \frac{1}{2}\partial_t \psi. \qquad (67)$$

In order to illustrate the procedure of asymptotic matching, a planar interface of a solid is considered that grows towards the positive x direction into a melt of initial dimensionless temperature $u(\infty) = -1 - \Delta$ with $0 < \Delta \ll 1$. It is easy to verify that the free-boundary problem has a steady-state solution: an interface propagating with a constant velocity $V = \beta\Delta$ and the temperature given by $u = -\Delta$ for $x < x_{int}$ and $u = -1 - \Delta + \exp[-(x - x_{int})V/D)]$ for $x > x_{int}$. The numerical solution of the phase-field model given by Eqs. (66) and (67) is plotted in Fig. 4 on the two relevant scales. On the outer scale (given by the diffusion length $l = D/V$), the phase-field profile appears as a sharp step, and the slope of the temperature field has an apparent discontinuity at the interface, as prescribed by the Stefan condition, Eq. (29). On the inner scale W, the slope of the temperature field changes slowly and continuously, since the source of latent heat is not concentrated in a single point, but "smeared out" over the entire interface region.

The two dash-dotted lines in Fig. 4b are fits to the asymptotes of the inner solution far from the interface, extrapolated to the interface position (the point where $\phi = 0$). This is an illustration of the matching condition between inner and outer

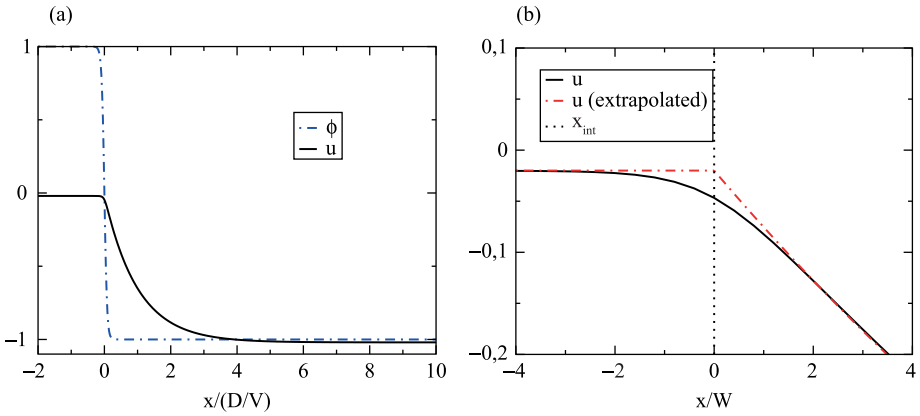

Figure 4: Steady-state solution of Eqs. (66) and (67) for Δ = 0.02 and λ = 1, plotted on the scale of the diffusion length *l* = D/V in (a) and on the scale of the interface thickness *W* in (b).

fields: the boundary conditions for the field u "seen" on the outer scale correspond to the values of these asymptotes at the interface. Note that (i) the two asymptotes reach the same value at the interface position, so that the temperature is continuous on the outer scale, and (ii) that the value of u at the intersection point (that is, the boundary condition on the outer scale) does not correspond to any value of the actual field u taken inside the interface.

The main result of the asymptotic calculations is that these equations are equivalent to the symmetric model of solidification, with

$$d_0 = a_1 \frac{W}{\lambda} \tag{68}$$

$$\beta = a_1 \left[\frac{\tau}{\lambda W} - a_2 \frac{W}{D} \right], \tag{69}$$

where $a_1 = 5\sqrt{2}/8$ and $a_2 = 0.6267$ are numbers of order unity. When other choices are made for f_{dw} and $g(\phi)$, the numbers a_1 and a_2 change, but the form of the equations remains the same as long as the symmetries of the functions remain the same $f_{dw}(-\psi) = f_{dw}(\psi)$ and $g(-\psi) = -g(\psi)$).

Equation (69) contains two terms: The first one is obtained if the temperature field is assumed to be constant inside the interface, and describes the dissipation due to a homogeneous undercooling of the interface. The second term is due to the inhomogeneities of the temperature field inside the interface, which are illustrated in Fig. 4b. It may seem surprising that this contribution plays an important role: the characteristic scale for the variations of the temperature field is the diffusion length, and therefore, an inhomogeneity on the scale of the interface should be unimportant if WV/D is small enough. However, this reasoning neglects the heat source term in Eq. (67): this term varies on the scale of W, and thus, always creates contributions to the diffusion field on that scale; therefore, the second term of Eq. (69) is important even for small velocities.[31]

The expression of the kinetic coefficient given by Eq. (69) is of crucial importance. Since there are two contributions of opposite sign, it is possible to choose $\beta = 0$, that is, to simulate interfaces in local equilibrium, with arbitrary interface thickness. The choice is limited, of course, by the convergence of the asymptotic matching procedure, which requires a sufficient separation between inner and outer scales. In practice, good convergence can often be obtained even with a scale ratio as large as 0.1.

3.6 *Application: Dendritic growth*

For the simulation of dendritic growth, surface energy anisotropy has to be included in the model. In the Karma-Rappel model, this can be achieved by letting the interface thickness W depend on the orientation $\hat{n}$ (which corresponds to the inclusion of anisotropy in the square gradient term),

$$W(\hat{n}) = \bar{W} a_c(\hat{n}). \tag{70}$$

The kinetic anisotropy can then be incorporated by choosing the orientation-dependent phase-field relaxation time by Eq. (69), which remains valid for anisotropic interfaces if W is replaced by its orientation-dependent value.[31]

The equation of motion for the phase field is modified by the presence of anisotropy; it now reads

$$\begin{aligned} \tau(\hat{n})\partial_t \psi = \bar{W}^2 \Bigg\{ \vec{\nabla} \Big(a_c(\hat{n})^2 \vec{\nabla} \psi \Big) \\ + \sum_{i=1}^{d} \partial_i \left[a_c(\hat{n}) \frac{\partial a_c(\hat{n})}{\partial(\partial_i \psi)} (\vec{\nabla} \psi)^2 \right] \Bigg\} \\ + \psi - \psi^3 - \lambda u (1 - \psi^2)^2 . \end{aligned} \tag{71}$$

The coordinate system is attached to the crystallographic axes of the growing monocrystal. For cubic materials, the anisotropy function that has been most extensively used is

$$a_c(\hat{n}) = 1 + \varepsilon_4 [4(n_x^4 + n_y^4 + n_z^4) - 3], \tag{72}$$

where ε_4 is the anisotropy strength; an equivalent expression holds for the kinetic anisotropy. In two dimensions, the interface orientation is described by a single angle θ, with $\hat{n} = (\cos\theta, \sin\theta)$, and we have simply $\gamma(\theta) = \bar{\gamma}[1 + \varepsilon_4 \cos(4\theta)]$. Simulations of dendritic growth have been carried out using this form of the anisotropy, and the results are in good agreement with solvability theory both at high[31,37] and low undercooling.[38] An example for such a dendrite is shown in Fig. 5. Good agreement with experiments has also been achieved concerning the anisotropic shape of the dendrite tip at low undercooling[38,39] and the growth velocity of Nickel dendrites at high undercooling.[40] This proves that a quantitative description of dendritic growth in a pure substance can be obtained with the help of the phase-field method.

Solvability theory: The currently accepted theory for the selection of the dendrite operating state. The name comes from the fact that a steady-state needle crystal solution of the free-boundary problem of crystal growth can only exist if the surface energy or the interface kinetics are anisotropic. The condition for the existence of a solution also yields an equation that determines the growth velocity.

3.7 *Phase-fied models for binary alloys*

The earliest attemps to formulate models for binary alloys just extended the formalism for a pure substance presented above[42,43] by making the free energies of solid and liquid depend on both T and c. The equation of motion for the number density of solute atoms, $\rho = c\bar{\rho}$, (a conserved quantity) is obtained by the standard variational procedure,

Figure 5: Dendrite simulated with the anisotropic Karma-Rappel model, with an anisotropy of the surface free energy given by Eq. (72) with $\varepsilon_4 = 0.00625$, and isotropic (vanishing) kinetics ($\beta(\hat{n}) = 0$). The dimensionless undercooling is $\Delta = 0.1$, that is, the initial and boundary values of $u = -0.1$. The simulation is carried out with the multi-scale algorithm described in Ref.[41]

$$\partial_t \rho = -\vec{\nabla} \cdot \vec{J} = \vec{\nabla} \cdot \left(M \frac{\delta F}{\delta \rho} \right), \tag{73}$$

where $\vec{J}$ is the solute flux and M is the atomic (chemical) mobility.

While this model is a viable representation of the physical system if the thickness of the phase-field interface has its natural (atomistic) width, it is difficult to use it with "upscaled" interfaces. The reason is that the interface properties intrinsically depend on the bulk thermodynamics in this model. This can be understood in several manners. As already found in Eq. (5), equilibrium between solid and liquid in a mixture implies that the function $\omega_v = f_v - \mu c_v$ takes the same values ω_{eq} for liquid and solid. Since the composition of solid and liquid in an alloy differ, this implies that there are two extensive quantities (f and c) that vary across the interface, in addition to the phase field ϕ. If Gibbs dividing surfaces are constructed by the condition of zero interface excesses for c, ϕ, and f, the positions of the three surfaces will in general not coincide. The profiles of ϕ and c at equilibrium are actually related, because the condition that the diffusion current vanishes yields

$$\frac{\delta F}{\delta \rho} = g(\varphi) \frac{\partial f_s}{\partial \rho} + (1 - g(\varphi)) \frac{\partial f_l}{\partial \rho} = \mu_{eq} = \text{const.} \tag{74}$$

This equation relates c and ϕ, and at a given point x within the interface, $g(\phi(x))\, f_s(\rho(x)) + [1 - g(\phi(x))]\, f_l(\rho(x)) - \mu\rho(x)$ generally differs from ω_{eq}. According to Eq. (8), this gives a contribution to the interface excess free energy γ. This fact was detected for the first time in Ref.[44]

Another way to reach the same insight is to write down the equilibrium condition for the phase field across a planar interface. It reads

$$0 = -\frac{\delta F}{\delta \phi} = K\partial_{xx}\phi - Hf'_{\mathrm{dw}}(\phi) + g'(\phi)[f_s(c,T) - f_l(c,T)]. \quad (75)$$

For a pure substance, the free energy densities of solid and liquid are equal; this is not the case for alloys. Therefore, in the interface (where $g'(\phi) \neq 0$) a driving force acts on the phase field that competes with the terms proportional to K and H to shape the interface profile. As a consequence, the surface free energy does not follow the simple scaling of Eq. (62), but also depends on the choice of the bulk free energies.

Different solutions have been developed to overcome this problem and to develop models in which the interface width can be more easily adjusted. The first idea was to start from a "phase-superposition" picture that is based on the general principles of volume-averaged transport equations for multi-phase systems.[45] Solid and liquid are seen as two independent macroscopic phases, with two separate composition fields c_s and c_l, which overlap in the diffuse interface region. This additional degree of freedom is removed by the condition that the diffusion potential of the two coexisting phases must be identical; for a dilute alloy, this is equivalent to the partition relation, $c_s = kc_l$. The equations of motion for the composition and the phase field are given in;[44] the combination $f - \mu\rho$ appears as the thermodynamic driving force for the phase field.

A completely equivalent formulation of this model can be written, in which the connection to the model for a pure substance is more straightforward.[14] It starts from the functional

$$\Omega = \int_V \omega_{\mathrm{int}} + \omega_s(\mu,T)g(\phi) + \omega_l(\mu,T)[1-g(\phi)]. \quad (76)$$

Here, ω_{int} has the same form as f_{int}, and $\omega_\nu = f_\nu - \mu\rho$ are, as in Eq. (18), the Legendre transforms of the free energy densities, which means that they depend on the diffusion potential instead of the composition. The equilibrium equation that result from the variation of this functional is equivalent to Eq. (75), with the difference $f_s - f_l$ replaced by $\omega_s - \omega_l$. Since the latter is zero at equilibrium, the interface profile is determined by ω_{int} alone, and the scaling of Eq. (62) applies, as desired.

Following exactly the same steps as for the development of the temperature equation in the pure substance model, an equation of motion for the diffusion potential is found,

$$\chi(\mu,T,\phi)\partial_t\mu = \vec{\nabla}(M\vec{\nabla}\mu) + (c_l - c_s)g'(\phi)\partial_t\phi, \quad (77)$$

with

$$\chi(\mu,T,\phi) = \chi_s(\mu,T)g(\phi) + \chi_l(\mu,T)[1-g(\phi)]$$
$$\chi_\nu = \frac{\partial^2\omega_\nu}{\partial\mu^2} \quad (78)$$

being a generalized susceptibility[24] that plays the same role as the specific heat in Eq. (54).

3.8 *Antitrapping current*

The model outlined above, as well as the models of Refs.[29,44] are still not suitable for the quantitative modelling of solidification microstructures with upscaled interfaces. The reason is the phenomenon of *solute trapping* already discussed in the sharp-interface context, which occurs during the solidification of alloys at sufficiently high velocity. Phase-field models can describe solute trapping quite well[46]: the transition from growth in local equilibrium to complete solute trapping with increasing growth velocity is well reproduced when the parameter WV/D is varied. However, the problem for quantitative simulations is quite obvious: since this effect depends on the thickness of the interface, its magnitude is greatly exaggerated if the interface thickness is upscaled in simulations. This means that solute trapping will appear for solidification velocities that are much smaller than those for which it is really observed in experiments. For accurate simulations, it has therefore, to be eliminated from the model.

A way to accomplish this was developed in Ref.[47] for isothermal solidification, and in Ref.[18] for directional solidification—an *antitrapping current* is added to the model. This is an additional contribution to the solute current which counteracts solute trapping. For this purpose, it should be proportional to the interface thickness and to the growth velocity, and it should be directed from the solid to the liquid in order to assist solute redistribution. Concretely, the solute current is written as

$$\vec{J} = -M\vec{\nabla}\tilde{\mu} + \vec{J}_{\mathrm{at}}, \quad (79)$$

with the antitrapping current

$$\vec{J}_{\mathrm{at}} = -a(\phi)(\rho_l - \rho_s)W\partial_t\phi\hat{n}, \quad (80)$$

where $a(\phi)$ is a dimensionless function of ϕ that depends on the details of the model, and $\rho_l - \rho_s$ is the concentration jump between the phases, taken at equilibrium. For the models of Refs.[18,47] that describe the solidification of dilute binary alloys, the function $a(\phi)$ is actually just a constant, the value of which has to be determined by matched asymptotic expansions. The details of this procedure can be found in Ref.[18]

3.9 *Application: Directional solidification of dilute binary alloys*

For dilute binary AB alloys, f_s and f_l may be assumed to be of the form of a regular solution model, taken in its dilute limit,

$$f_\nu(T,c) = f_\nu^A(T) + \varepsilon_\nu c + \frac{RT}{V_m}\left(c\ln c - c\right), \quad (\nu = s,l) \tag{81}$$

where $f_s^A(T)$ and $f_l^A(T)$ are the free energy densities of pure A, ε_s and ε_l are constants with dimension energy per unit volume, R is the ideal gas constant, and the last term in Eq. (81) is the dilute limit of the entropy of mixing. A standard calculation of the solid-liquid equilibrium yields that the partition relation is satisfied for dilute concentrations, $c_s = kc_l$ for $c_l, c_s \ll 1$, with the partition coefficient k given by

$$k = \exp\left(\frac{V_m(\varepsilon_l - \varepsilon_s)}{RT_m}\right), \tag{82}$$

and that the liquidus in the phase diagram is a straight line of slope

$$m = \frac{RT_m^2(1-k)}{LV_m}. \tag{83}$$

Here, T_m and L are the melting temperature and latent heat of melting of the pure solvent (A atoms).

The models of Refs.[18,47] can be obtained from these free energies following the procedure outlined above and by introducing the variable

$$U = \frac{\rho(\phi,\mu) - \rho_{\mathrm{eq}}(\phi)}{(1-k)\rho_{\mathrm{eq}}(\phi)}, \tag{84}$$

that generalizes the variable U introduced in Eq. (42), where $\rho(\phi,\mu) = -\partial\omega(\phi,\mu)/\partial\mu$, and $\rho_{eq}(\phi,\mu)$ its equilibrium value at some reference temperature T_{eq}. After some algebra,[14,18] and going through the same steps as listed above for the Karma-Rappel model, the equations take the form

$$\tau\left[1-(1-k)\frac{z-V_pt}{l_T}\right]\frac{\partial\psi}{\partial t} = W^2\nabla^2\phi + \phi - \phi^3 - \lambda g'(\phi)\left(U + \frac{z-V_pt}{l_T}\right), \tag{85}$$

$$\left(\frac{1+k}{2} - \frac{1-k}{2}h(\psi)\right)\frac{\partial U}{\partial t} = \vec{\nabla}\cdot\left(Dq(\psi)\vec{\nabla}U + \frac{1}{2\sqrt{2}}W\left[1+(1-k)U\right]\frac{\partial\psi}{\partial t}\frac{\vec{\nabla}\psi}{|\vec{\nabla}\psi|}\right) + \left[1+(1-k)U\right]\frac{1}{2}\frac{\partial h(\psi)}{\partial t}. \tag{86}$$

Here, D is the solute diffusivity in the liquid, and $q(\psi) = (1-\psi)/2$ an interpolation between 0 in the solid and 1 in the liquid (one-sided model). These equations are valid for directional solidification with a constant pulling velocity V_p, contain the

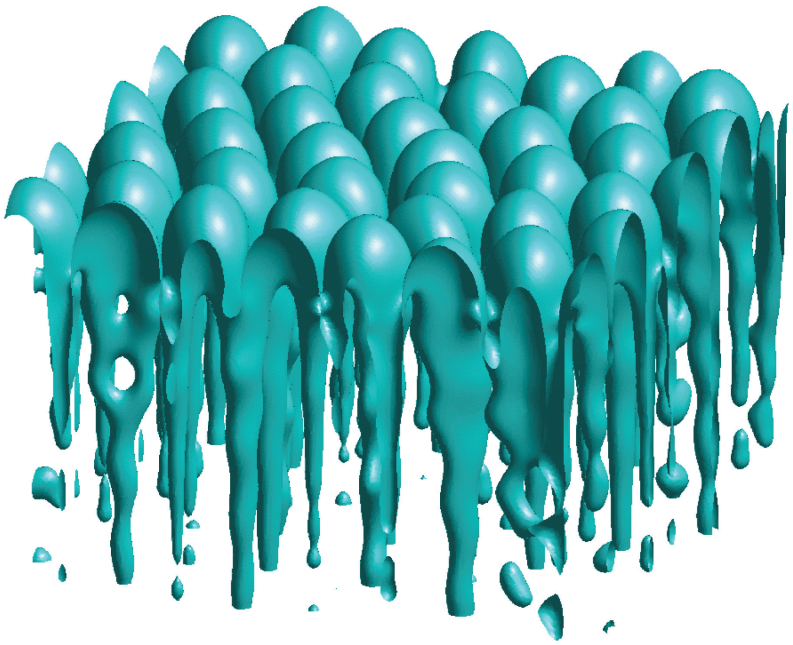

Figure 6: Cellular solidification front simulated with the anisotropic dilute binary alloy phase-field model. The cross-section of the simulation domain is 240 × 240 grid points. For details, see Ref.[53]

antitrapping current, and are non-variational in the same respect as the Karma-Rappel model: the function $g(\psi)$ has been replaced by $h(\psi)$ in the evolution equation for U.

The detailed asymptotic analysis presented in Ref.[18] has demonstrated that this set of equations is indeed equivalent to the sharp-interface problem of alloy solidification given by Eqs. (43) to (45). The simulations presented in[18,47] were the first examples for a successful interface upscaling in phase-field modelling of alloy solidification. Since then, this methodology has been used to explore dendritic and cellular solidification in alloys, and convincing quantitative agreement between simulations, theories, and experiments has been achieved.[48–52] An example for a simulation of a three-dimensional cellular solidification front, taken from Ref.[53] is shown in Fig. 6. The antitrapping methodology has also been extended to other alloy models.[14,15,54,55]

4 Conclusions and Perspectives

Here, the exposition was limited to two simple phase-field models: the symmetric model for pure-substance solidification and the one-sided model for dilute binary alloy solidification. It should be clear that the methodologies can be applied in a straightforward manner to more complicated problems. Here, only a small choice of references can be given. First, binary alloys models can be generalized to arbitrary phase diagrams,[14,44] with a coupling to CALPHAD databases if necessary.[56] Second, recently progress was made on a re-formulation of the antitrapping concept[57–59] that opens the perspective of quantitative modelling of solidification with arbitrary diffusivity ratios.[60,61] Third, multicomponent alloys can be treated by coupling the phase-field equation to a multicomponent diffusion model. An asymptotic analysis and an antitrapping formulation have been published.[54] Fourth, multiple phases and/or grains can also be treated using the multi-phase-field method.[62–64] General models for multi-phase and multi-component solidification have been put forward,[15,55] but careful benchmark simulations remain to be done to assess their precision. A model that combines the symmetric and one-sided models for thermal and solute diffusion has also been developed[65] and used to explore thermosolutal dendritic growth.[66] Finally, melt convection can also be added.[29]

Beyond solidification, phase-field models can also be applied for the simulation of many other phenomena that involve the development of complex interfacial patterns; reviews on the use of such models in solid-state phase transformations[67] and two-phase flow[68] are available. From its origins in the physical description of phase transitions, the phase-field method has grown today into a versatile and useful tool for materials scientists and engineers.

Received 4 July 2016.

References

1. M.C. Cross and P.C. Hohenberg, *Rev. Mod. Phys.* **65**, 851 (1993).
2. J.S. Langer, *Rev. Mod. Phys.* **52**, 1 (1980).
3. W. Kurz and D.J. Fisher, Fundamentals of Solidification, *Trans Tech Publications*, Zurich, Switzerland, 1998.
4. M. Asta, C. Beckermann, A. Karma, W. Kurz, R. Napolitano, M. Plapp, G. Purdy, M. Rappaz and R. Trivedi, *Acta Mat.* **57**, 941–971 (2009).
5. J.A. Dantzig and M. Rappaz, Solidification, EPFL Press, Lausanne, 2009.
6. N. Provatas and K. Elder, Phase-field methods in materials science and engineering, Wiley-VCH, Weinheim, 2010.
7. M. Plapp, in: T. Nishinaga (Ed.), The Handbook of Crystal Growth, 2nd edition, Vol. 1B, Elsevier, Amsterdam, 2015, pp. 631–668.
8. J.J. Hoyt, M. Asta and A. Karma, *Mat. Sience Eng. R* **41**, 121 (2003).
9. K.-A. Wu, A. Karma, J.J. Hoyt and M. Asta, *Phys. Rev. B* **73**, 094101 (2006).
10. J. Stefan, Sitzungsberichte der Österreichischen Akademie der Wissenschaften Mathematisch-Naturwissenschaftliche Klasse, Abteilung 2, Mathematik, Astronomie, Physik, Meteorologie und Technik **98**, 965–983 (1889).
11. J. Stefan, Annalen der Physik und Chemie **42**, (1891) 269–286.
12. A. Visintin, in: C. Dafemos and M. Pokorny (Eds.), Handbook of Differential Equations: Evolutionary Differential Equations vol. IV, Amsterdam, pp. 377–484.
13. P. Nozières, in: C. Godrèche (Ed.), Solids far from equilibrium, Edition Aléa Saclay, Cambridge University Press, Cambridge, UK, 1991, pp. 1–154.
14. M. Plapp, *Phys. Rev. E* **84**, 031601 (2011).
15. A. Choudhury and B. Nestler, Phys. Rev. E **85**, 021602 (2012).
16. K.-A. Wu, C.-H. Wang, J.J. Hoyt and A. Karma, *Phys. Rev. B* **91**, 014107 (2015).
17. M.J. Aziz and J. Appl. *Phys.* **53**, 1158 (1982).
18. B. Echebarria, R. Folch, A. Karma and M. Plapp, *Phys. Rev. E* **70**, 061604 (2004).
19. J.S. Langer, in: G. Grinstein and G. Mazenko (Eds.), Directions in Condensed Matter Physics, World Scientific, Singapore, 1986, pp. 165–186.
20. G.J. Fix, in: A. Fasano and M. Primicerio (Eds.), Free boundary problems: Theory and applications, Piman, Boston, 1983, p. 580.
21. J.B. Collins and H. Levine, *Phys. Rev. B* **31**, 6119–6122 (1985).
22. J.S. Rowlinson, *J. Stat. Phys.* **20**, 197–244 (1979).

CALPHAD: CALPHAD stands for CALculation of PHAse Diagrams. It is a systematic method to obtain approximations for the free energy of alloys by fitting a large class of model functions to all available data (from experiments and simulations).

23. P.C. Hohenberg and B.I. Halperin, *Rev. Mod. Phys*. **49**, 435–479 (1977).
24. J.S. Langer, in: C. Godrèche (Ed.), Solids far from equilibrium, Edition Aléa Saclay, Cambridge University Press, Cambridge, UK, 1991, pp. 297–363.
25. Q. Bronchart, Y. L. Bouar and A. Finel, *Phys. Rev. Lett.* **100**, 015702 (2008).
26. J.J. Hoyt, M. Asta and A. Karma, *Phys. Rev. Lett*. **86**, 5530–5533 (2001).
27. P.M.D. Bedeaux and A.M. Albano, *Physica A* **82**, 438–462 (1976).
28. B. Caroli, C. Caroli and B. Roullet, in: C. Godrèche (Ed.), Solids far from equilibrium, Edition Aléa Saclay, Cambridge University Press, Cambridge, UK, 1991, pp. 155–296.
29. C. Beckermann, H.-J. Diepers, I. Steinbach, A. Karma and X. Tong, *J. Comput. Phys.* **154**, 468 (1999).
30. Y. Sun and C. Beckermann, *Physica D* **198**, 281 (2004).
31. A. Karma and W.-J. Rappel, *Phys. Rev. E* **57**, 4323–4349 (1998).
32. G. Caginalp and P. Fife, *Phys. Rev. B* **34**, 4940–4943 (1986).
33. G.B. McFadden, A.A. Wheeler, R.J. Braun, S.R. Coriell and R.F. Sekerka, *Phys. Rev. E* **48**, 2016–2024 (1993).
34. R. Kobayashi, *Physica D* **63**, 410–423 (1993).
35. R.F. Almgren, *SIAM J. Appl. Math*. **59**, 2086–2107 (1999).
36. M. Plapp, in: R. Mauri (Ed.), Multiphase microfluidics: The Diffuse Interface Model, Springer, Wien, 2012, pp. 129–175.
37. A. Karma, W.-J. Rappel and *J. Cryst. Growth* **174**, (1997) 54–64. 10th American Conference on Crystal Growth/9th International Conference on Vapor Growth and Epitaxy, VAIL, CO, AUG 04–09, 1996.
38. A. Karma, Y. H. Lee and M. Plapp, *Phys. Rev. E* **61**, 3996–4006 (2000).
39. J.C. LaCombe, M.B. Koss, V.E. Fradkov and M.E. Glicksman, *Phys. Rev. E* **52**, 2778–2786 (1995).
40. J. Bragard, A. Karma, Y.H. Lee and M. Plapp, *Interface Science* **10**, 121–136 (2002).
41. M. Plapp, A. Karma and *J. Comput. Phys*. **165**, 592 (2000).
42. A.A. Wheeler, W.J. Boettinger and G. B. McFadden, *Phys. Rev. A* **45**, 7424–7439 (1992).
43. G. Caginalp and W. Xie, *Phys. Rev. E* **48**, 1897–1909 (1993).
44. S.G. Kim, W.T. Kim and T. Suzuki, *Phys. Rev. E* **60**, 7186–7197 (1999).
45. J. Ni and C. Beckermann, *Met. Trans. B* **22**, 349–361 (1991).
46. N.A. Ahmad, A.A. Wheeler, W.J. Boettinger and G.B. McFadden, *Phys. Rev. E* **58**, 3436 (1998).
47. A. Karma, *Phys. Rev. Lett*. **87**, 115701 (2001).
48. M. Greenwood, M. Haataja and N. Provatas, *Phys. Rev. Lett*. **93**, 246101 (2004).
49. S. Gurevich, A. Karma, M. Plapp and R. Trivedi, *Phys. Rev. E* **81**, 011603 (2010).
50. B. Echebarria, A. Karma and S. Gurevich, *Phys. Rev. E* **81**, 021608 (2010).
51. N. Bergeon, D. Tourret, L. Chen, J.-M. Debierre, R. Guérin, A. Ramirez, B. Billia, A. Karma and R. Trivedi, *Phys. Rev. Lett*. **110**, 226102 (2013).
52. D. Tourret, J.M. Debierre, Y. Song, F.L. Mota, N. Bergeon, R. Guerin, R. Trivedi, B. Billia and A. Karma, *Phys. Rev. E* **92**, (2015).
53. Y. Ma, M. Plapp and J. Cryst. growth **385**, 140–147 (2014). 7th International Workshop on Modeling in Crystal Growth, Taipei, TAIWAN, OCT 28–31, 2012.
54. S.G. Kim, Acta Materialia **55**, 4391–4399 (2007).
55. I. Steinbach, Model. *Simul. Mater. Sci. Eng.* **17**, 073001 (2009).
56. I. Steinbach, B. Boettger, J. Eiken, N. Warnken and S.G. Fries, Journal of Phase Equilibria and Diffusion **28**, 101–106 (2007). Symposium on Multi-Component Alloy Thermodynamics, San Antonio, TX, MAR 12–16, 2006.
57. E. A. Brener, G. Boussinot, *Phys. Rev. E* **86**, (2012).
58. G. Boussinot and E. A. Brener, *Phys. Rev. E* **88**, (2013).
59. A. Fang and Y. Mi, *Phys. Rev. E* **87**, (2013).
60. M. Ohno and K. Matsuura, *Phys. Rev. E* **79**, 031603 (2009).
61. M. Ohno, T. Takaki and Y. Shibuta, *Phys. Rev. E* **93**, (2016).
62. I. Steinbach, F. Pezzolla, B. Nestler, M. Seeßelberg, R. Prieler, G.J. Schmitz and J.L.L. Rezende, *Physica D* **94**, 135–147 (1996).
63. J. Tiaden, B. Nestler, H.-J. Diepers and I. Steinbach, *Physica D* **115**, 73–86 (1998).
64. R. Folch and M. Plapp, *Phys. Rev. E* **72**, 011602 (2005).
65. J.C. Ramirez, C. Beckermann and A. Karma, H.-J. Diepers, *Phys. Rev. E* **69**, 051607 (2004).
66. J.C. Ramirez and C. Beckermann, *Acta Mater.* **53**, 1721–1736 (2005).
67. L.-Q. Chen, *Annu. Rev. Mater. Res*. **32**, 113 (2002).
68. D.M. Anderson, G.B. McFadden and A.A. Wheeler, *Annual Review of Fluid Mechanics* **30**, 139 (1998).

Mathis Plapp After studies of physics at University of Freiburg, Germany, and University of Paris Sud, France, Mathis Plapp obtained his Ph.D. from Ecole Polytechnique, France. He spent two years as a postdoctoral fellow at Northeastern University, Boston, USA, and then became a permanent staff member at Centre National de Recherche Scientifique, France. Since 2006, he is also professor at the physics department of Ecole Polytechnique. Since 2015, he directs the Condensed Matter Physics laboratory at Ecole Polytechnique.